Wind Energy

WIND ENERGY
Wind Energ. (2016)
Published online in Wiley Online Library (wileyonlinelibrary.com). DOI: 10.1002/we.2076

RESEARCH ARTICLE

Prediction of wind-turbine fatigue loads in forest regions based on turbulent LES inflow fields

B. Nebenführ[1,2] and L. Davidson[1,2]

[1] Division of Fluid Dynamics, Department of Applied Mechanics, Chalmers University of Technology, Gothenburg, Sweden
[2] Swedish Wind Power Technology Centre (SWPTC), Chalmers University of Technology, Gothenburg, Sweden

ABSTRACT

Large-eddy simulations (LES) were used to predict the neutral atmospheric boundary layer over a sparse and a dense forest, as well as over grass-covered flat terrain. The forest is explicitly represented in the simulations through momentum sink terms. Turbulence data extracted from the LES served then as inflow turbulence for the simulation of the dynamic structural response of a generic wind turbine. In this way, the impact of forest density, wind speed and wind-turbine hub height on the wind-turbine fatigue loads was studied. Results show for example significantly increased equivalent fatigue loads above the two forests. Moreover, a comparison between LES turbulence and synthetically generated turbulence in terms of load predictions was made and revealed that synthetic turbulence was able to excite the same spectral peaks as LES turbulence but lead to consistently lower equivalent fatigue loads. Copyright © 2016 John Wiley & Sons, Ltd.

KEYWORDS
fatigue loads; wind turbine; forest canopy; large-eddy simulation; atmospheric turbulence

Correspondence
L. Davidson, Chalmers University of Technology, Applied Mechanics, SE-41296 Gothenburg, Sweden.
E-mail: lada@chalmers.se

Received 4 May 2015; Revised 6 November 2016; Accepted 9 November 2016

1. INTRODUCTION

Forest regions are becoming an increasingly interesting environment for the placement of wind turbines. It is often easier to develop a wind park in a forest region than for sites near residential areas, as the forest helps to mitigate the visible and audible effects of the wind turbines. Consequently, permits for developing a wind park are often more easily granted for forest regions. Usually, the wind resource above forests provides for poor wind-power production, as mostly low wind speeds are encountered. However, wind-turbine towers of 100 m or more allow for effective wind-turbine operation even in this environment. Additionally, maintenance and grid connection are simplified compared with offshore wind parks, owing to existing infrastructure. Unfortunately, the wind resource above forests is characterized by strong turbulence and large wind shear, imposing strong fluctuating aerodynamic loads and strong cyclic loading on the turbines. Since design criteria for modern wind turbines are not adapted to forest conditions, the strong loading is expected to negatively influence the fatigue life of modern wind turbines. In order to avoid much wind-turbine downtime, it is necessary to understand the implications of the forest-induced loads on the turbine.

Traditionally, the wind-turbine fatigue life has been investigated by load simulations based on synthetically generated turbulence. However, the International Electrotechnical Commission (IEC) guidelines[1] for example require rather simplified inflow turbulence characteristics compared with real-life atmospheric boundary layers (ABL). Only neutral stratification is considered, along with a power-law velocity profile and a constant wind-shear exponent. In real ABL flows, the turbulence is usually generated at (or near) the bottom surface and transported upwards. Consequently, the turbulence intensity decreases with increasing height, while the IEC synthetic turbulence only contains a constant turbulence intensity over the entire swept rotor area. Furthermore, synthetic turbulence does not account for wind veer (different wind directions at different heights), while this phenomenon is always present in the ABL and is usually most pronounced in stable stratification[2,3] ; for a comprehensive review of the typical simplifications of synthetic turbulence, refer to Park *et al.*[4]

More advanced synthetic turbulence models have been developed, such as the one proposed by Mann,[5,6] where effects of complex terrain have also been considered by Mann.[7] Chougule *et al.*[8] have included the effects of a forest and thermal

stratification in terms of a curve-fitting approach. Most recently, Segalini and Arnqvist[9] modified the Mann model in order to account for the effects of thermal stratification. However, as a next step towards more realistic turbulence conditions, large-eddy simulation (LES) can be considered for the generation of wind turbine inflow field generation. Physical phenomena, such as Coriolis force, thermal stratification, complex terrain (e.g. forest canopies) and height dependence of the turbulence intensity, are inherently included and will be represented in the simulation results. LES has proven to be a valuable tool for the simulation of the ABL under stable,[10–12] neutral[13,14] and unstable conditions.[13,15] Even simulations of a full diurnal cycle have successfully been carried out with LES.[16] Moreover, complex terrain in terms of the Askervein hill was studied by Bechmann and Sørensen,[17] and flows in and above forest canopies[2,18–23] have been considered. Despite its potential, so far only few researchers have attempted to use LES for wind turbine inflow generation. Sim *et al*.[24] focused on neutral stratification, while Churchfield *et al*.[25] also included the effects of unstable conditions. Stable stratification was investigated by Park *et al*.[4] While Sim *et al*.[24] and Park *et al*.[4] were saving a database of turbulence fields for use as inflow for a structural wind-turbine simulator, Churchfield *et al*.[25] employed an integrated approach by coupling LES and the structural wind-turbine simulator FAST (Fatigue, Aerodynamics, Structures and Turbulence).[26]

Here, we use LES to compute the air flow over three different types of terrain: a dense forest, a sparse forest and grass-covered flat terrain. To allow for a comparison between different wind speeds, datasets are extracted from each of the simulations and scaled to the desired hub-height wind speed. The structural wind-turbine simulator FAST[26] is used to predict the loads on the NREL 5MW reference wind turbine,[27] based on inflow turbulence from LES. Eventually, the influence of the forest and the forest density on the loads is explored, along with an analysis of the impact of the hub-height wind speed. The assumption that higher wind-turbine towers can be used to reduce the turbulence-induced loads is tested in Section 4.5.

2. INFLOW TURBULENCE GENERATION

In LES, turbulent structures are distinguished into large, resolvable scales and small, subgrid scales that require modelling. This distinction is carried out implicitly by the grid and is usually referred to as grid filtering. We solve the incompressible, grid-filtered Navier–Stokes equations and a transport equation for small, subgrid scales turbulent kinetic energy, which is used to provide a velocity scale for modelling the smallest eddies. The simulation method is described in detail in Nebenführ and Davidson.[2,22] As we consider only neutral stratification here, the transport equation for potential temperature is not solved.

The forest is explicitly included in the simulations through a source term in the momentum equations. Following Shaw and Schumann,[18] this source term reads,

$$F_{f,i} = -C_D a_f U u_i, \tag{1}$$

where C_D denotes a forest drag value set to 0.15,[28] a_f is the vertical leaf-area density of the forest and U is the local velocity magnitude. A right-handed coordinate system is used, where coordinates x, y and z point in the streamwise, lateral and vertical directions, respectively.

In order to compare the influence of the forest canopy on the fatigue loads of wind turbines, we carry out three simulations with different forest densities: a sparse forest, a dense forest and a case without forest. Using the empirical model of Lalic and Mihailovic,[29] the leaf-area density profiles, depicted in Figure 1, were generated. The leaf-area density profiles are computed directly at the grid points. It can be seen that the leaf-area density profiles represent trees with a more dense crown region and a less obstructed trunk space. In the case without forest, $a_f = 0$ for all height levels and consequently $F_{f,i} = 0$. An overall impression of the forest density is given by the leaf-area index,

$$A = \int_0^h a_f(z) dz, \tag{2}$$

where h is the canopy height. The three forest density profiles correspond to leaf-area indices of $A \approx 4.3$, $A \approx 2.9$ and $A = 0.0$ for the dense, sparse and no forest cases, respectively. The most dense profile is identical to the one that proved successful in LES for a test site in Ryningsnäs in southeastern Sweden.[2,22] At Ryningsnäs, the forest consists predominantly of Scots pine trees (*Pinus silvestris*).[30,31]

At the ground, the momentum flux is specified from standard similarity theory; the local wind speed, $U = \sqrt{u^2 + v^2}$, at the first vertical grid point, $\Delta_z/2$, is used for evaluation of the surface momentum flux, viz.

$$\tau_{i3,w} = -\left[\frac{U_{par}\kappa}{\ln[(\Delta_z/2)/z_0]}\right]^2 \frac{u_i(x, y, \Delta_z/2)}{U}, (i = 1, 2), \tag{3}$$

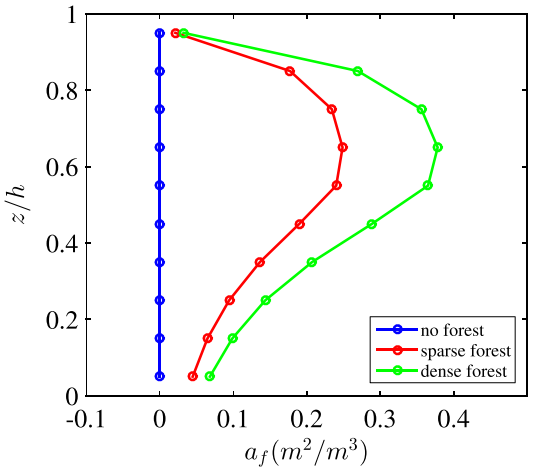

Figure 1. Leaf-area density profiles used in the three simulations. The symbols indicate the vertical grid points and the respective leaf-area density values.[Colour figure can be viewed at wileyonlinelibrary.com]

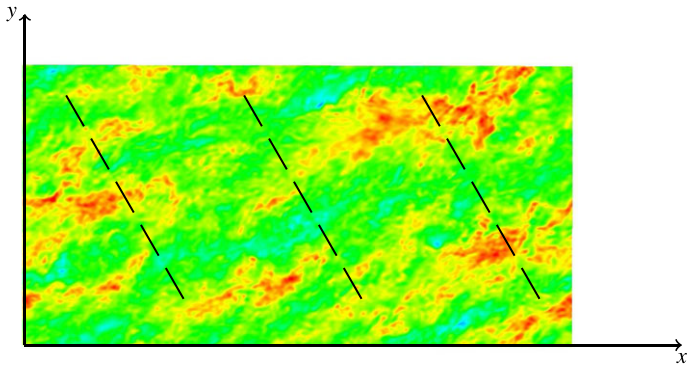

Figure 2. An example of the instantaneous flow field at the hub height and a schematic view of the locations of turbulence extraction planes (▬▬).[Colour figure can be viewed at wileyonlinelibrary.com]

where $\kappa = 0.41$ denotes the von Kármán constant and $z_0 = 0.001h$ is the aerodynamic roughness length at the ground according to Shaw and Schumann.[18] The top of the domain is treated as a rigid, frictionless lid, and periodic boundary conditions are employed in the x-direction and y-direction. It can be seen that the case without forest yields a simulation of a rough-wall boundary layer over the low aerodynamic roughness specified by z_0. With the given canopy height, the simulated surface represents a grass-covered landscape[32,33] : conditions similar to the ones often found near onshore wind turbines.[4] For the simulations, an incompressible finite-volume based LES code[34] is used, which is of second-order accuracy in space and time. The simulations are performed on a rectangular domain with dimensions of $2000 \times 1000 \times 1000$ m^3. A grid with $384 \times 192 \times 96$ cells is used to discretize the computational domain. The grid spacing is constant in the horizontal directions with $\Delta_x = \Delta_y = 5.2$ m. The forest density varies with height, as depicted in Figure 1, but is assumed to be homogeneous in the horizontal directions. A canopy height of $h = 20$ m is used in the simulations throughout the paper. Ten grid cells are used to discretize the canopy in the vertical direction, yielding a constant grid spacing of $\Delta_z = 2$ m inside the forest. Above a height of $z = 40$ m, the cells are geometrically stretched by 4%. In all simulations, a desired wind speed of 12 m s^{-1} at 90 m above ground is specified. At each timestep, the large-scale pressure gradient in the horizontal directions, required to maintain the specified wind speed, is calculated. A constant timestep of $\Delta_t = 0.2$ s is used in all simulations, which ensures that the Courant number is below 0.5 in the entire domain.

After the simulations have reached their quasi-steady state*, consecutive datasets of a duration of 1000 s are extracted with a frequency of 5 Hz on cut planes covering the entire swept rotor area of the National Renewable Energy Laboratory

*The quasi-steady state was assessed manually by following the time history of the velocity at several heights (most importantly at the top of the ABL). As soon as both wind direction and mean wind speed did not change in magnitude anymore, the quasi-steady state is reached.

(NREL) 5MW onshore wind turbine.[27] We use cut planes of 41×41 grid points with a spacing of $\Delta_\eta = \Delta_\psi = 4$ m, where η and ψ denote the lateral and vertical directions in the local cut plane coordinate system, respectively. The cut planes are centred around the wind turbine hub height in the vertical and lateral directions.

As a consequence of the Coriolis effect incorporated in the LES, the wind direction changes with height. Here, the cut planes are extracted perpendicular to the mean wind direction at hub height of the wind turbine, as shown in Figure 2. This will allow for load calculations free of yaw-angles but still includes the effects of wind veer over a rotor diameter. Fifteen spatially non-overlapping datasets are extracted simultaneously, with the extraction planes being placed in three rakes with a displacement of 500 m in x-direction. Each rake contains five side-by-side extraction planes. Even though the datasets are not overlapping in space, some of them are partly overlapping in time. In order to investigate the effect of hub-height wind speed on the fatigue loads and to obtain comparable data for the three different cases, the datasets are also scaled to hub-height wind speeds of 8 and 16 m s^{-1}. With 45 datasets for each of the three forest densities simulated, we are able to compare 15 datasets per wind speed and forest density. Additional datasets of synthetic turbulence for a hub-height wind speed of 12 m s^{-1} are also included in the analysis. These are generated using the TuGEN code,[35] which generates synthetic inflow turbulence based on the Mann model.[5,6] Input parameters are chosen according to the recommendations given by Chougule *et al.*[8] for the Ryningsnäs test site in neutral stratification. The mean wind profile is described as a power law with a constant shear exponent of $\alpha = 0.42$, deduced from the LES (while the IEC standard would require $\alpha = 0.2$[1]).

3. FATIGUE-LOAD SIMULATIONS USING FAST

The aeroelastic wind-turbine response to the various inflow conditions was simulated using the software FAST[26] that is developed and provided by the NREL. FAST can be employed for analysing two-bladed or three-bladed horizontal-axis wind turbines, which can be equipped with either a downstream or an upstream rotor. Both onshore and fixed or floating offshore wind turbines can be considered. FAST uses a combined modal/multibody representation of the wind turbine in the time domain. Rigid and flexible bodies are interrelated with a number of degrees of freedom. Both the tower, the blades and the driveshaft are assumed to be flexible, while the support platform at the ground and all other components are assumed to be rigid. The tower and blades are described with the help of linear mode shapes that need to be calculated a priori. The driveshaft is modelled as a linear torsional spring and damper. The aerodynamic forces on the rotor are evaluated through a blade-element momentum method and are based on the input flow fields from the LES. At each timestep, the turbulent inflow plane is updated from the stored LES data. Collective pitch and variable-speed torque control algorithms are available for the simulation of the wind-turbine dynamic response to the inflow turbulence.

Structural and material information and airfoil data were taken from the NREL 5MW reference wind turbine in its onshore configuration,[27] which is completely openly available. It is a three-bladed, horizontal-axis wind turbine with an upstream rotor orientation, delivering a rated power of 5MW. The hub height is 90 m, and the blades have a length of 63 m. The structural information for the turbine is summarized in Table I, and the complete structural and aerodynamical description is available in Jonkman *et al.*[27]

It should be noted here that the fatigue-load simulations are carried out for a total of 930 s. However, the first 330 s are discarded, which yields 10 min time series. This is carried out in order to ensure that the initial transient has disappeared from the time histories of the fatigue load.

Table I. Details of the NREL 5MW Reference Wind Turbine.[27]

Rated power	5 MW
Rotor orientation	Upstream
Number of blades	3
Cut-in wind speed	3.0 m s^{-1}
Rated wind speed	11.4 m s^{-1}
Cut-out wind speed	25.0 m s^{-1}
Cut-in rotor speed	6.9 rpm
Rated rotor speed	12.1 rpm
Rotor diameter	126 m
Hub height	90 m
Control	Collective pitch control
	Variable-speed torque control

4. RESULTS AND DISCUSSION

Here, we consider three typical turbine loads for the analysis: the fore-aft bending moment in the base of the tower (TBBM), the flapwise (normal to rotor plane) bending moment in the root of one blade (BRBM) and the low-speed shaft bending moment (LSSBM) around the lateral axis. The latter is taken as a measure for the load on the main shaft bearing.

4.1. LES flow results

Spatially and temporally averaged LES results for the two with-forest cases are evaluated against field measurements from southeastern Sweden[30] in Figure 3. The normalized wind-speed profiles are presented in Figure 3(a). Both forest densities are in good agreement with the measurements but deviate from each other above $z/h \approx 7$. As expected, the denser forest leads to a stronger flow retardation inside the canopy.

The normalized vertical momentum flux in streamwise direction is shown in Figure 3(b), and it can be seen that the two simulated cases overestimate the momentum flux above the forest. From its maximum right above the forest, the momentum flux will decay linearly to zero at the upper end of the ABL. The different decay rates indicate that the boundary-layer height in the simulations is different from the thickness of the ABL in the field measurements. Additionally, the wind turning due to Coriolis forces may be underestimated in the simulations, which also would lead to different momentum flux decay rates. Inside the canopy, the momentum sink term (1) makes the momentum flux vanish rapidly.

Figure 4 shows a comparison of the wind-speed profile and the turbulence intensity obtained from the three simulations. It can clearly be seen in Figure 4(a) that the wind shear is significant for the forest cases than for the non-forest case. Moreover, the turbulence intensity is more than doubled by the presence of a forest. Consequently, considerably higher wind turbine fatigue loads can be expected for the with-forest cases.

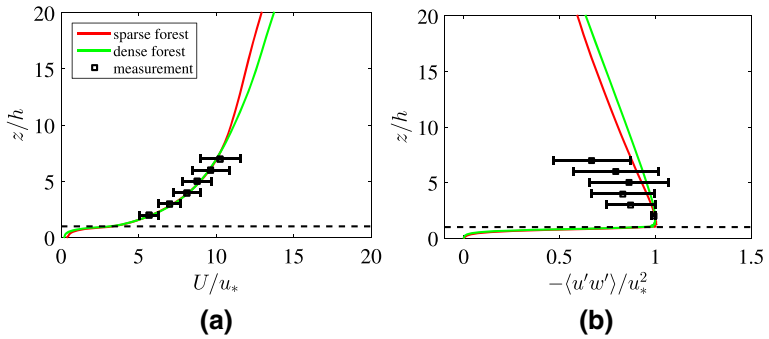

Figure 3. Spatially and temporally averaged simulation results compared with field measurements in southeastern Sweden. (a) wind-speed profile and (b) momentum flux profile. The black dashed line marks the top of the canopy.[Colour figure can be viewed at wileyonlinelibrary.com]

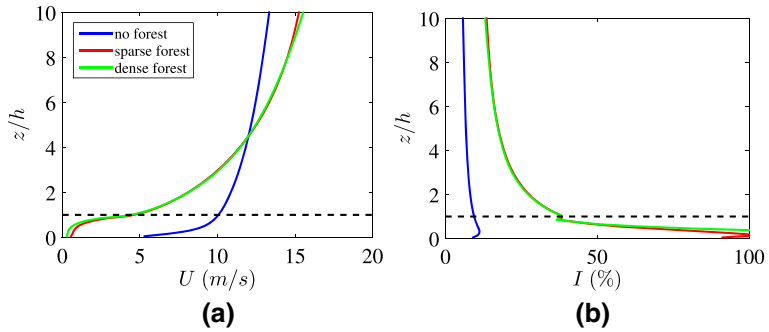

Figure 4. Spatially and temporally averaged results from the three simulations. (a) wind-speed profile and (b) turbulence intensity. The black dashed line marks the top of the canopy.[Colour figure can be viewed at wileyonlinelibrary.com]

4.2. Comparison of LES turbulence and synthetic turbulence

The direct comparison of two 10 min time series is given in Figure 5(a), showing that, while the large-scale fluctuations appear similar for both techniques, the synthetically generated turbulence contains more high-frequency, small-scale fluctuations than the time series from LES. Figure 5(b) displays the power-spectral density of the hub-height turbulence for the two turbulence generation techniques. Both spectra follow a $-5/3$ decay, but LES turbulence exhibits a significant drop in energy at frequencies greater than $f_c \approx 0.35$ Hz, while the synthetic turbulence starts to drop at higher frequencies. The limiting factor in the LES is the grid resolution in the numerical domain, and here the cut-off frequency can be approximated by u_{RMS}/Δ_x. As of today, it is not feasible to generate LES turbulence with much higher cut-off frequencies; for example, a cut-off frequency of 1 Hz would require grid refinement by a factor 25 in the horizontal plane, i.e. Δ_x and Δ_y need to be of the order of 1 m.

Similar results are obtained for the spectra of BRBM, TBBM and LSSBM for load calculations based on synthetic turbulence and turbulence from LES, as presented in Figure 6. Generally speaking, the loads based on LES tend to be larger and therefore yield somewhat higher energy in the spectra. For all three loads, spectral peaks are clearly visible, and they are simulated similarly in terms of frequency, regardless of the inflow turbulence generation method. Once again, LES turbulence leads to somewhat higher energy content in the peaks. In Figure 6(b), the spectral peaks correspond to the rotor rotational frequency (1P) and its two higher harmonics (2P, 3P). As reported by Churchfield *et al.*,[25] the fact that the peak of 1P is the largest indicates that the strongest bending moment is associated with the cyclic loading of the blade due to wind shear. Once in each revolution, the blade is subjected to high and low wind speed, respectively. The LSSBM feels the collective load of all three blades, and therefore, the peak loads are shifted to three times higher frequencies (3P, 6P, 9P) than for the single blade bending moment as shown in Figure 6(c). Three times in each revolution of the rotor, one of the blades will be exposed to the highest bending moment (due to high wind speed in the upwards blade position). This implies that the wind shear is the most important quantity, also for the bending of the low-speed shaft. Good representation of the peaks

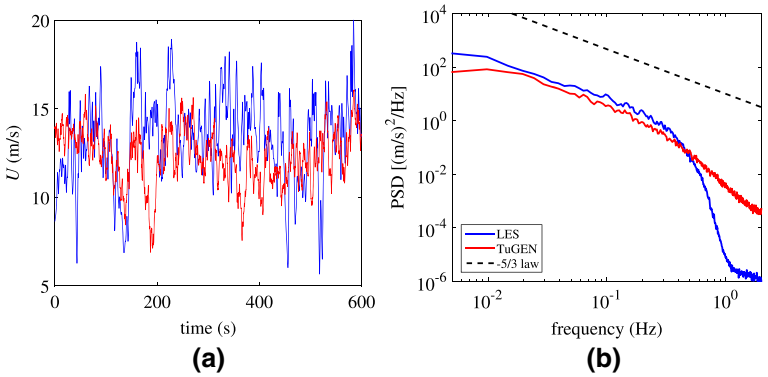

Figure 5. (a) Ten minute time-history and (b) power-spectral density of the wind speed at hub height from the two different inflow generation techniques.[Colour figure can be viewed at wileyonlinelibrary.com]

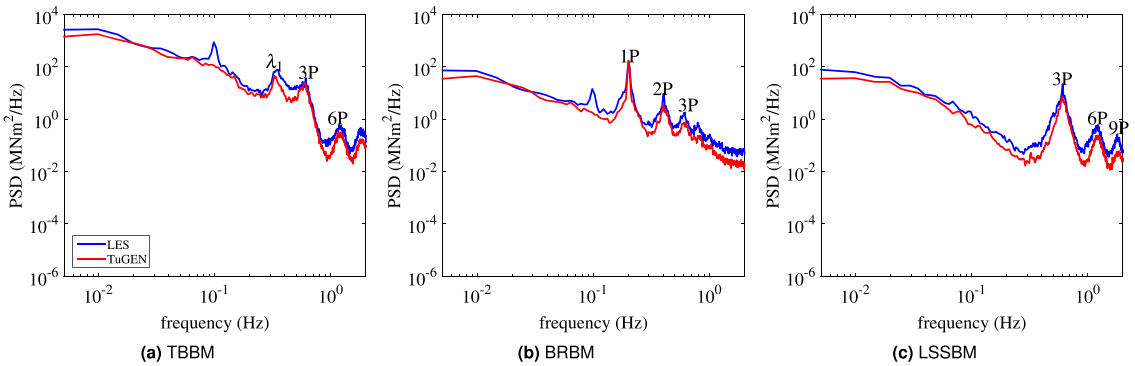

Figure 6. Comparison of spectra of TBBM, BRBM and LSSBM for $U_{Hub} = 12$ m s^{-1} over a sparse forest. Results are averaged over 15 realizations.[Colour figure can be viewed at wileyonlinelibrary.com]

DOI: 10.1002/we

at 1P, 2P, 3P, etc., is usually achieved as a consequence of the rotational sampling due to the blade motion, as also reported by Sim *et al.*[24] In Figure 6(a), yet another peak can be identified at a frequency of $\lambda_1 \approx 0.33$ Hz, corresponding to the first natural fore-aft frequency of the wind-turbine tower.[27] Previous work has shown this peak to be largely underpredicted, when load calculations were based on LES turbulence,[24] caused by too low a cut-off frequency in the wind-speed spectra. These authors mitigated the problem by means of a fractal interpolation technique, which helped to add high-frequency content to their low-frequency LES turbulence.[36] Underprediction of this spectral peak may lead to considerable errors in the prediction of the entire wind-turbine fatigue life. Here, the cut-off frequency in the wind spectra (Figure 5(b)) is comparable with the first natural frequency of the tower, and therefore, it is possible to excite the fore-aft tower bending motion. It should be noted that this is far from universal and that in order to excite the first natural frequency of a smaller wind turbine (with a higher natural frequency), higher cut-off frequencies would be required. An additional peak is visible at approximately 0.1 Hz in Figure 6(a) and (b). The cause of this peak is not known, and its cause should be investigated in a future study, alongside with its impact on the wind-turbine fatigue loads.

Figure 7 displays box-and-whiskers plots of the mean values of the TBBM, BRBM and LSSBM obtained from 15 realizations based on LES and synthetic turbulence, where the box represents the middle half of the data, while the whiskers outside the box stand for the lower and upper quartiles of the data. The line inside the box marks the median value. Therefore, the entire plot gives an impression of the sample-to-sample variability of the results. Load calculations based on LES turbulence tend to give smaller mean and median values than calculations based on synthetic turbulence, except for the LSSBM. However, the spread of the results from realization to realization is considerably larger in the LES case, which might indicate that the LES is resolving low-frequency phenomena that are not included in the synthetic turbulence.

A rain-flow counting algorithm[37] was employed in order to produce the fatigue loads histograms in Figure 8. The EFL is calculated as

$$EFL = \left(\sum_{i=1}^{N_c} \frac{S_i^m}{N_0} \right)^{1/m}, \tag{4}$$

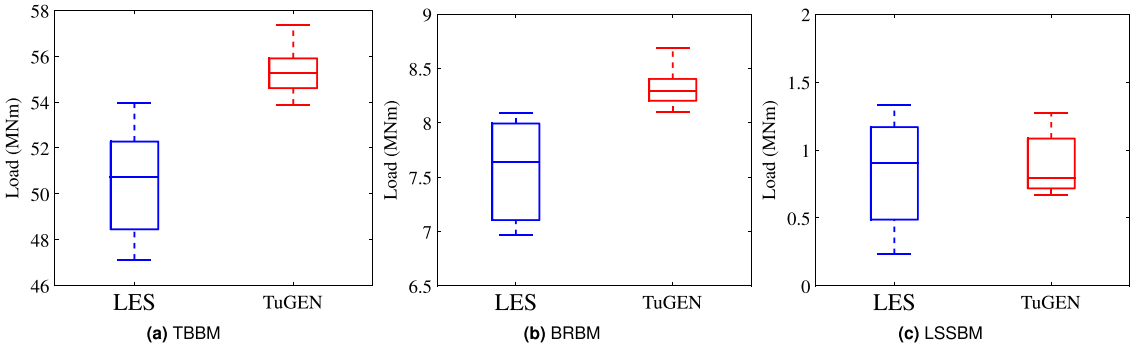

Figure 7. Mean values of TBBM, BRBM and LSSBM based on inflow turbulence from LES and TuGEN for a hub-height wind speed of 12 m s^{-1} above the sparse forest. Results are averaged over 15 realizations.[Colour figure can be viewed at wileyonlinelibrary.com]

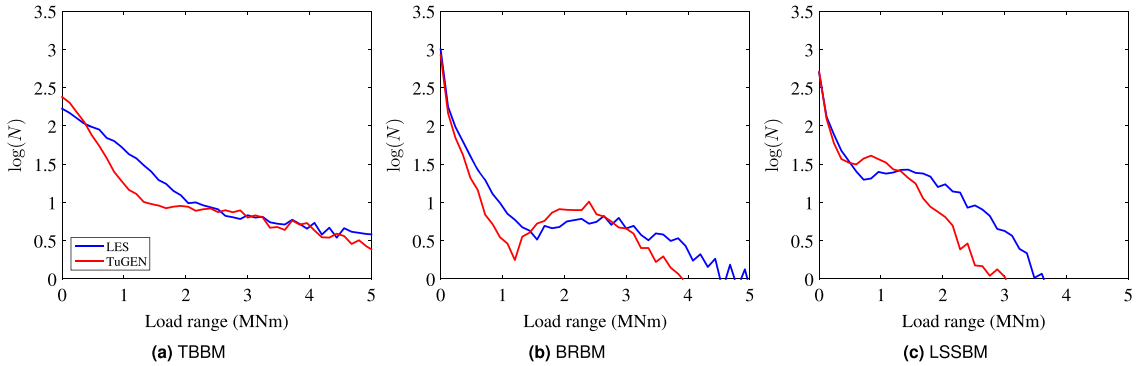

Figure 8. Comparison of fatigue load histograms of TBBM, BRBM and LSSBM based on inflow turbulence from LES and TuGEN for $U_{Hub} = 12$ m s^{-1} above the sparse forest. Results are averaged over 15 realizations.[Colour figure can be viewed at wileyonlinelibrary.com]

where N_c is the number of effective load cycles, S_i are the load amplitudes, m is the Wöhler exponent, taken as 3 for the steel tower and the low-speed shaft and as 10 for the composite material of the blades, and N_0 is the equivalent number of cycles representing 10 min (here, $N_0 = 600$ corresponding to 1 Hz). The EFL and the effective number of cycles are given in Table II. Somewhat larger number of cycles and larger loads can generally be identified from the load simulations based on LES inflow turbulence, which is also reflected in the calculated EFLs.

Turbulence from LES tends to give higher loads than the synthetic turbulence, which is probably caused by the higher hub-height turbulence intensity found in the LES data. However, due to the lack of real-life measurements, it is difficult to evaluate which inflow turbulence results in the more realistic loads. It is noteworthy that we considered the least challenging case for the synthetic turbulence by choosing neutral stability. In stable or unstable conditions, the benefits of LES over synthetic turbulence are likely to become more obvious, as synthetic turbulence is often only poorly adapted to these conditions.

4.3. Influence of forest density

The mean values of the loads from 15 representations are plotted in box-and-whiskers plots in Figure 9. The median of the TBBM only slightly increases with increasing forest density, while a significant change is obtained for the LSSBM from the without-forest to the with-forest cases. In particular for the LSSBM, also the variability between different representations is significantly increased for the with-forest cases. However, the median of the TBBM and the BRBM in the without-forest case is higher than in the with-forest cases. A possible explanation is the lower wind shear in the without-forest case, which reduces the cyclic loading on the blades, but the blades experience a larger bending moment even in the 180°azimuthal position (where 0°is vertically upward).

The presence of the forest leads to higher fatigue loads, as shown in the fatigue load histograms in Figure 10 and Table III. It can be seen that the without-forest case yields slightly higher cycles of the smallest loads than the with-forest cases. However, the load range is more than doubled in the presence of a forest with significant number of cycles in the range above 2 MNm. The forest density itself appears to be of little influence on the loads. The EFLs are almost tripled by the presence of a forest, and the denser forest yields a slightly higher EFL than the sparse forest for the TBBM, indicating that increasing forest density has a slightly negative effect on the wind-turbine fatigue life. One interpretation of this is that summer is the most harmful season for wind turbines placed in decidious forests, since the trees are then fully leaved and thus most dense. Largely increased loads were reported for forest regions by Ganander and Carlén[38] in a study based on synthetic turbulence and by Nebenführ and Davidson for LES turbulence-based load calculations.[23]

Table II. EFL and effective cycles. Results are averaged over 15 realizations.

	TBBM		BRBM		LSSBM	
Input	EFL [MNm]	N_c	EFL [MNm]	N_c	EFL [MNm]	N_c
LES	6.0	1370	3.5	1582	1.7	1170
TuGen	4.3	1189	2.7	1273	1.1	1091

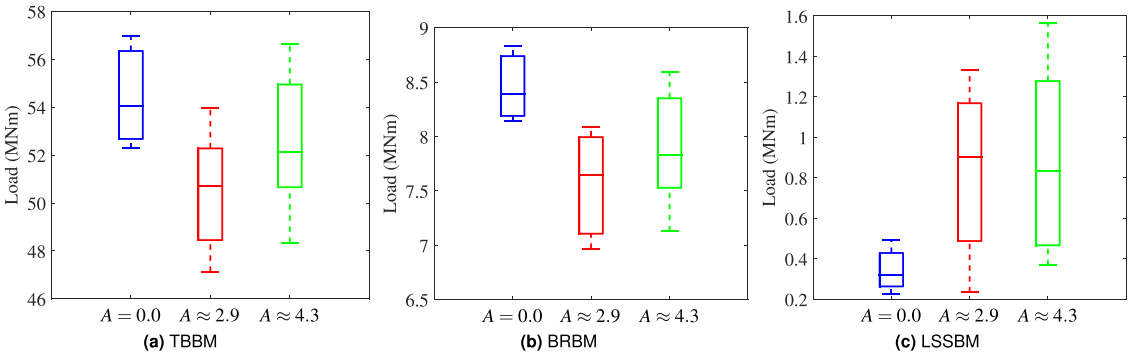

Figure 9. Mean values of TBBM, BRBM and LSSBM for a hub-height wind speed of 12 m s^{-1} with varying forest density. Results are averaged over 15 realizations.[Colour figure can be viewed at wileyonlinelibrary.com]

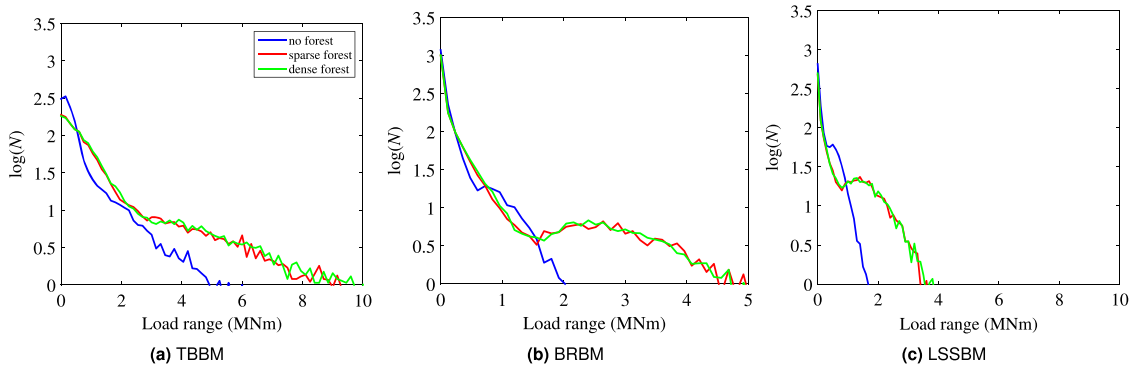

Figure 10. Influence of the forest density on the fatigue-load histograms of TBBM, BRBM and LSSBM for a hub-height wind speed of 12 m s^{-1}. Results are averaged over 15 realizations.[Colour figure can be viewed at wileyonlinelibrary.com]

Table III. EFL and effective cycles.

	TBBM		BRBM		LSSBM	
Input	EFL (MNm)	N_C	EFL (MNm)	N_C	EFL (MNm)	N_C
LAI= 0	2.6	1425	1.4	1689	0.6	1308
LAI= 2.9	6.0	1370	3.5	1582	1.7	1107
LAI= 4.3	6.2	1393	3.5	1604	1.7	1198

Results are averaged over 15 realizations.

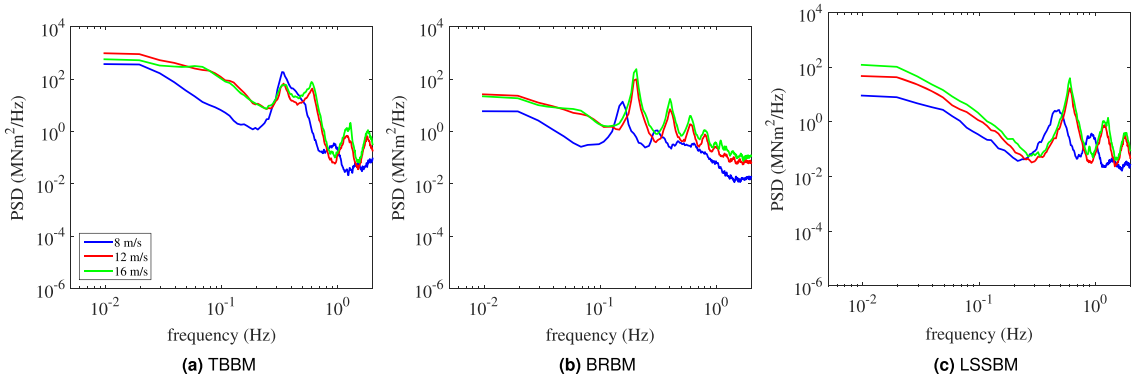

Figure 11. Power-spectral density of TBBM, BRBM and LSSBM for the sparse forest with varying hub-height wind speed. Results are averaged over 15 realizations.* [Colour figure can be viewed at wileyonlinelibrary.com]

4.4. Influence of wind speed

Here, we investigate the influence of the wind speed on the loads above the sparse forest. Figure 11 displays the power-spectral density of the three loads for the different wind speeds considered. As shown in Figure 11(a), the first natural frequency of the tower seems more strongly excited at $U_{Hub} = 8$ m s^{-1} than for higher wind speeds. At this hub-height wind speed, the rotor runs at a rotational rate of about 9.2 rpm, translating into a frequency of approximately 0.15 Hz. This is roughly half the natural frequency of the tower, and it is possible that the blade passings cause resonance in the tower. Moreover, owing to the lower rotational rate of the rotor, all other spectral peaks are moved towards lower frequencies, since the rotational sampling happens more slowly.

Again, the mean values of the loads are represented by box-and-whiskers plots in Figure 12. It becomes clear that the TBBM and BRBM are the highest in wind speeds of 12 m s^{-1}. At hub-height wind speeds higher than that, the

*Note that 40% of the FAST simulations failed for the lowest hub-height wind speed. Therefore, the results for the lowest wind speed are averaged over nine realizations, instead of 15.

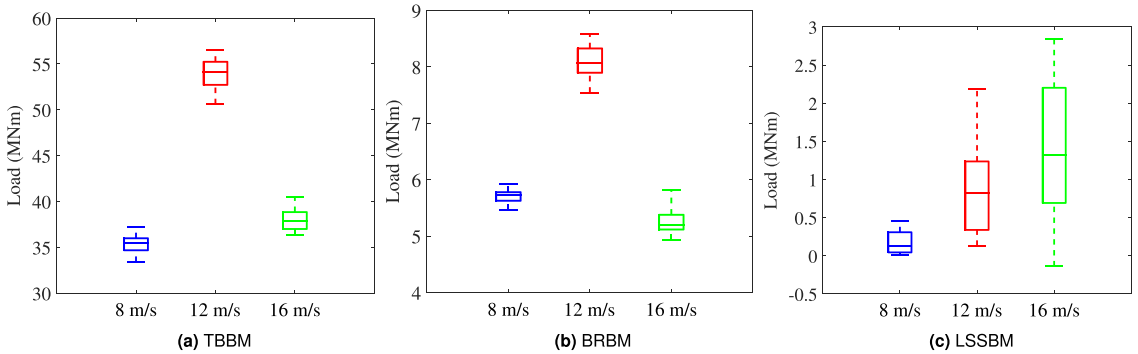

Figure 12. Mean values of TBBM, BRBM and LSSBM for the sparse forest with varying hub-height wind speed. Results are averaged over 15 realizations.[Colour figure can be viewed at wileyonlinelibrary.com]

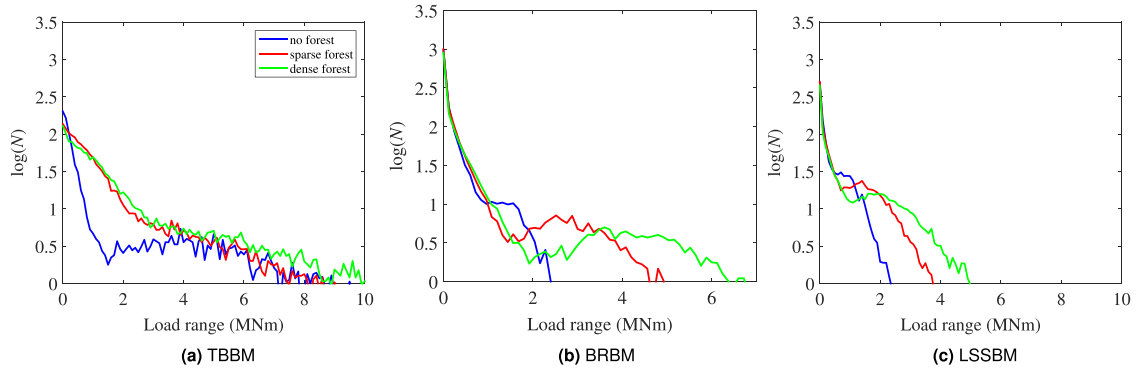

Figure 13. Influence of the wind speed on the fatigue-load histograms of the BRBM for the sparse forest. Results are averaged over 15 realizations.[Colour figure can be viewed at wileyonlinelibrary.com]

Table IV. EFL and effective cycles. Results are averaged over 15 realizations.

	TBBM		BRBM		LSSBM	
Input	EFL (MNm)	N_c	EFL (MNm)	N_c	EFL (MNm)	N_c
$U_{Hub} = 8$ m s^{-1}	4.6	876	1.6	1474	0.9	1076
$U_{Hub} = 12$ m s^{-1}	5.5	1428	3.6	1596	1.7	1211
$U_{Hub} = 16$ m s^{-1}	6.5	1431	4.9	1493	2.4	1160

wind-turbine control system starts pitching the blades in order to reduce the loads, resulting in the load reduction at $U_{Hub} = 16$ m s^{-1}. This observation is confirmed by the findings of Sim *et al.*[24] and Agarwal.[39] On the contrary, the LSSBM is constantly increasing with increasing wind speed, indicating that the control algorithm should be improved in order to better protect the main bearing.

In Figure 13 and Table IV, one can deduce that increasing wind speeds lead to amplified fatigue loads. An increasing number of cycles, in particular of the large loads, appear for the higher wind speeds, leading to an increased EFL.

It should be noted that the FAST simulations for the lowest wind speed failed in about 40% of the cases in forest conditions due to too large blade deflection and the subsequent violation of the underlying small angle assumption. This did not happen for the without-forest cases, suggesting that large coherent structures or strong individual wind gusts appear in the inflow turbulence over the forest, which are absent over the low-roughness surface. Since no extreme gusts were found in the time history of the hub-height wind speed, for the time of the failure, it is likely that a large coherent structure is responsible for the behaviour. For the higher wind speeds, no failures appeared, indicating that the large blade deflections could be handled by the wind turbines blade-pitch control. At wind speeds below rated, the blade-pitch controller is not usually active, and its activation appears to happen too late (or too slowly) to react on the strong turbulence over a forest. Using LIDAR measurements, it is possible to obtain information about the incoming turbulence before it hits the wind

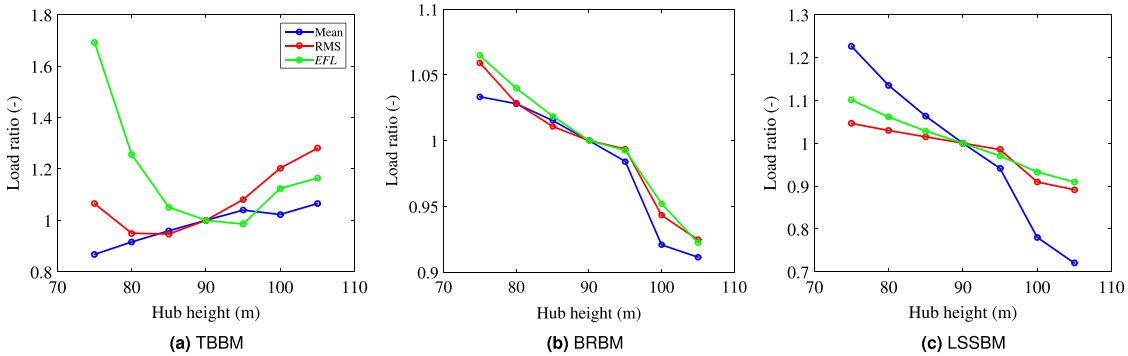

Figure 14. Influence of the hub height on the mean, RMS and EFL values of the TBBM, BRBM and LSSBM for a wind speed of 12 m s^{-1} at 90 m above the sparse forest. All values are normalized with their respective value at the original hub height of 90 m. Results are averaged over 15 realizations.[Colour figure can be viewed at wileyonlinelibrary.com]

turbine. This information can be used for preventively pitching the blades, when strong wind gusts are detected ahead of the wind turbine. Recently, such predictive wind-turbine control strategies have been developed,[40,41] and as the wind resource in forest regions is usually restricted to fairly low wind speeds (below rated), the potential of these novel control strategies may be huge.

4.5. Influence of hub height

Often, the use of higher wind-turbine towers is mentioned in relation to reducing the fatigue loads, when operating wind turbines in a forest region. The expected reduction in fatigue loads is due to lower turbulence levels at greater heights. In order to test that claim, we have used the turbulence datasets from the sparse forest with a wind speed of 12 m s^{-1} at 90 m and ran FAST simulations for hub heights of 75, 80, 85, 90, 95, 100 and 105 m while keeping all other settings the same. Figure 14 shows the evolution of the mean (blue), RMS (red) and EFL (green) values of the TBBM, BRBM and LSSBM in relation to their respective value at the original hub height of 90 m. While the mean value of the TBBM steadily increases with increasing hub height—mainly as a consequence of the larger lever—the EFL does not increase significantly for greater hub heights. However, for the 75 and 80 m large towers, the EFL of the TBBM is seen to increase considerably. For the BRBM and the LSSBM, a trend can be seen towards lower loads with increasing hub height, which confirms the common assumption. As an example, a reduction of 7% and 10% could be expected for the EFL of the BRBM and LSSBM, respectively, by increasing the hub height from 90 to 105 m.

5. CONCLUSION

Large-eddy simulations were used for predicting the airflow over two simplified forests and a flat low-roughness surface at neutral stratification. From the numerical simulations, a number of turbulence datasets were extracted for subsequent use as inflow turbulence in the structural wind-turbine simulator FAST. As a reference and in order to assess the feasibility of LES as an inflow generator, load simulations based on synthetically generated turbulence using the Mann model were also studied. Besides investigating the influence of the forest density and the hub-height wind speed, the influence of the grid resolution of the inflow plane for the load simulations is also examined. Load simulations were carried out for the NREL 5MW reference wind turbine and the TBBM, the BRBM and the LSSBM were chosen for comparison.

Firstly, it could be shown that turbulence from LES is capable of producing comparable loads with synthetically generated turbulence. Of particular importance is that the first natural frequency of the tower could also be excited by the LES turbulence, which had not been carried out before. Here, this was achieved with a grid resolution of 5.2×5.2 m^2 in the horizontal direction, leading to a cut-off frequency of about 0.35 Hz, which is slightly above the tower first natural frequency. It should therefore be noted that for smaller wind turbines with a higher natural frequency of the tower, a higher grid resolution (and a higher cut-off frequency) may be needed. Even though the synthetic turbulence was generated according to parameters fitted to the forest in Ryningsnäs,[8] the hub-height turbulence intensity was found to be lower than that of the LES turbulence, leading to smaller loads in comparison. Whether this is an effect of accounting for physical phenomena such as wind veer and variable wind shear in the LES remains an open issue.

Secondly, the presence of a forest was found to increase the wind-turbine equivalent fatigue loads by a factor of three for the BRBM. With increasing forest density, a slight increase of the EFLs was noticed, indicating that summer may be the most hazardous season for wind turbines in decidious forests, because of the full leaf cover. It was shown that the median of the mean values increased for the LSSBM above a forest, while the presence of a forest reduced the mean values of the TBBM and the BRBM.

The wind speed was found to increase the loads up to 12 m s^{-1}. Above that, the wind-turbine control system starts pitching the blades and thereby reduces the loads. However, the LSSBM constantly increased with increasing wind speed, suggesting that the control algorithm should be improved to better protect the main bearing. Forest conditions in combination with the hub-height wind speed of 8 m s^{-1} were found to cause failure of the FAST simulations in about 40% of the cases. It seems as if the blade pitch controller is not responding sufficiently quickly to the incoming turbulence, leading to large blade deflections. As low wind speeds are often encountered above forests, this may potentially prove to be harmful for wind turbines installed in a forest environment.

Studying the influence of the hub height on the fatigue loads confirmed the common assumption that higher wind-turbine towers lead to a load reduction. For the sparse forest, the EFL of the BRBM and LSSBM could be reduced by 7% and 10%, respectively, simply by increasing the wind-turbine hub height from 90 to 105 m.

ACKNOWLEDGEMENTS

This project is financed through the Swedish Wind Power Technology Centre (SWPTC). SWPTC is a research centre for the design of wind turbines. The purpose of the centre is to support Swedish industry with knowledge of design techniques as well as maintenance in the field of wind power. The Centre is funded by the Swedish Energy Agency, Chalmers University of Technology as well as academic and industrial partners.

REFERENCES

1. IEC, Wind turbine-part 1: Design requirements, IEC 61400-1, *Technical Report*, International Electrotechnical Commission, Geneva, Switzerland, 2005.
2. Nebenführ B, Davidson L. Large-eddy simulation study of thermally stratified canopy flow. *Boundary-Layer Meteorology* 2015; **156**: 253–276.
3. Nebenführ B. Turbulence-resolving simulations for engineering applications, *PhD Thesis*, Chalmers University of Technology, Göteborg, 2015.
4. Park J, Basu S, Manuel L. Large-eddy simulation of stable boundary layer turbulence and estimation of associated wind turbine loads. *Wind Energy* 2014; **17**: 359–384.
5. Mann J. The spatial structure of neutral atmospheric surface-layer turbulence. *Journal of Fluid Mechanics* 1994; **273**: 141–168.
6. Mann J. Wind field simulation. *Probabilistic Engineering Mechanics* 1998; **13**: 269–282.
7. Mann J. The spectral velocity tensor in moderately complex terrain. *Journal of Wind Engineering and Industrial Aerodynamics* 2000; **88**: 153–169.
8. Chougule A, Mann J, Segalini A, Dellwik E. Spectral tensor parameters for wind turbine load modeling from forested and agricultural landscapes. *Wind Energy* 2015; **18**: 469–481.
9. Segalini A, Arnqvist J. A spectral model for stably stratified turbulence. *Journal of Fluid Mechanics* 2015; **781**: 330–352.
10. Basu S, Porté-Agel F. Large-eddy simulation of stably stratified atmospheric boundary layer turbulence: a scale-dependent dynamic modeling approach. *Journal of the Atmospheric Sciences* 2006; **63**: 2074–2091.
11. Beare RJ, Macvean MK, Holtslag AA, Cuxart J, Esau I, Golaz JC, Jimenez MA, Khairoutdinov M, Kosovic B, Lewellen D, Lund TS, Lundquist JK, Mccabe A, Noh Y, Raasch S, Sullivan P. An intercomparison of large-eddy simulations of the stable boundary layer. *Boundary-Layer Meteorology* 2006; **118**: 247–272.
12. Zhou B, Chow FK. Turbulence modeling for the stable atmospheric boundary layer and implications for wind energy. *Flow, Turbulence and Combustion* 2012; **88**: 255–277.
13. Deardorff JW. Numerical investigation of neutral and unstable planetary boundary layers. *Journal of the Atmospheric Sciences* 1972; **29**: 91–115.
14. Porté-Agel F, Meneveau C, Parlange MB. A scale-dependent dynamic model for large-eddy simulation: application to a neutral atmospheric boundary layer. *Journal of Fluid Mechanics* 2000; **415**: 261–284.
15. Sullivan PP, Patton EG. The effect of mesh resolution on convective boundary layer statistics and structures generated by large-eddy simulation. *Journal of the Atmospheric Sciences* 2011; **68**: 2395–2415.

16. Basu S, Vinuesa JF, Swift A. Dynamic LES modeling of a diurnal cycle. *Journal of Applied Meteorology and Climatology* 2008; **47**: 1156–1174.
17. Bechmann A, Sørensen NN. Hybrid RANS/LES method for wind flow over complex terrain. *Wind Energy* 2010; **13**: 36–50.
18. Shaw RH, Schumann U. Large-eddy simulation of turbulent flow above and within a forest. *Boundary-Layer Meteorology* 1992; **61**: 47–64.
19. Dupont S, Brunet Y. Influence of foliar density profile on canopy flow: a large-eddy simulation study. *Agricultural and Forest Meteorology* 2008; **148**: 976–990.
20. Dupont S, Bonnefond JM, Irvine MR, Lamaud E, Brunet Y. Long-distance edge effects in a pine forest with a deep and sparse trunk space: *in situ* and numerical experiments. *Agricultural and Forest Meteorology* 2011; **151**: 328–344.
21. Bohrer G, Katul GG, Walko RL, Avissar R. Exploring the effects of microscale structural heterogeneity of forest canopies using large-eddy simulations. *Boundary-Layer Meteorology* 2009; **132**: 351–382.
22. Nebenführ B, Davidson L. Influence of a forest canopy on the neutral atmospheric boundary layer—a LES study. *Etmm10: 10th International Ercoftac Symposium on Turbulence Modelling and Measurements, 17-19 September, 2014*, Marbella, Spain, 2014.
23. Nebenführ B, Carlén I, Caracoglia L, Davidson L. Development of a reduced-order model for wind turbine response to atmospheric turbulence in forest regions. In *Proceedings of 6th International Symposium on Computational Wind Engineering, 8–12 June, 2014*: Hamburg, Germany, 2014.
24. Sim C, Basu S, Manuel L. On space-time resolution of inflow representations for wind turbine loads analysis. *Energies* 2012; **5**: 2071–2092.
25. Churchfield MJ, Lee S, Michalakes J, Moriarty PJ. A numerical study of the effects of atmospheric and wake turbulence on wind turbine dynamics. *Journal of Turbulence* 2012; **13**: N14.
26. Jonkman J M, Buhl Jr M L, FAST user's guide, *Technical Report* NREL/EL-500-29798, National Renewable Energy Laboratory, Golden, Colorado, 2005.
27. Jonkman JM, Butterfield S, Musial W, Scott G. *Definition of a 5-MW reference wind turbine for offshore system development*. National Renewable Energy Laboratory: Golden, CO, 2009.
28. Shaw RH, Den Hartog G, Neumann HH. Influence of foliar density and thermal stability on profiles of Reynolds stress and turbulence intensity in a deciduous forest. *Boundary-Layer Meteorology* 1988; **45**: 391–409.
29. Lalic B, Mihailovic DT. An empirical relation describing leaf-area density inside the forest for environmental modeling. *Journal of Applied Meteorology* 2004; **43**(4): 641–645.
30. Bergström H, Alfredsson H, Arnqvist J, Carlén I, Dellwik E, Fransson J, Ganander H, Mohr M, Segalini A, Söderberg S. Wind power in forests: wind and effects on loads. *Vindforsk Rapport* 2013: 1–167.
31. Arnqvist J, Dellwik E, Segalini A, Bergström H. Wind statistics from a forested landscape. *Boundary-Layer Meteorology* 2015; **156**(1): 53–71.
32. Wieringa J. Updating the Davenport roughness classification. *Journal of Wind Engineering and Industrial Aerodynamics* 1992; **41**: 357–368.
33. Wieringa J. Representative roughness parameters for homogeneous terrain. *Boundary-Layer Meteorology* 1993; **63**(4): 323–363.
34. Davidson L, Peng SH. Hybrid LES-RANS modelling: a one-equation SGS model combined with ak–ω model for predicting recirculating flows. *International Journal for Numerical Methods in Fluids* 2003; **43**: 1003–1018.
35. Gilling L, TuGen: Synthetic turbulence generator, manual and user's guide, *Technical Report*, Department of Civil Engineering, Aalborg University, 2009.
36. Basu S, Foufoula-Georgiou E, Porté-Agel F. Synthetic turbulence, fractal interpolation, and large-eddy simulation. *Physical Review E* 2004; **70**: 026310.
37. ASTM, Standard practices for cycle counting in fatigue analysis, *Technical Report*, ASTM-E1049-85, American Society for Testing and Materials, West Conshohocken, PA, 1985.
38. Ganander H, Carlén I, Fatigue loading of wind turbines operating in forest terrain, *Technical Report*, TG-R-12-11: Teknikgruppen AB, Täby, Sweden, 2012.
39. Agarwal P. Structural reliability of offshore wind turbines, *PhD Thesis*, University of Texas, Austin, 2008.
40. Laks J, Pao L. Y, Simley E, Wright A, Kelley N, Jonkman B. Model predictive control using preview measurements from LIDAR. *Proceedings of 49th AIAA Aerospace Sciences Meeting*, Orlando, Fla, 2011.
41. Schlipf D, Schlipf DJ, Kühn M. Nonlinear model predictive control of wind turbines using LIDAR. *Wind Energy* 2013; **16**: 1107–1129.